Coordination Numbers in Sm Doped Ceria Using X-ray Absorption Spectroscopy

Julius Koettgen[*,†,‡,¶,§] and Manfred Martin[*,†,‖,⊥,‡]

†*Institute of Physical Chemistry, RWTH Aachen University, Landoltweg 2, 52056 Aachen, Germany*

‡*JARA-HPC, Forschungszentrum Jülich and RWTH Aachen University, Germany*

¶*Materials Sciences Division, Lawrence Berkeley National Laboratory, Berkeley, California 94720, United States*

§*Department of Materials Science and Engineering, University of California, Berkeley, California 94720, United States*

‖*Helmholtz-Institut Münster (IEK-12), Forschungszentrum Jülich GmbH, Corrensstr. 46, 48149 Münster, Germany*

⊥*JARA-Energy, Forschungszentrum Jülich and RWTH Aachen University, Germany*

E-mail: julius.koettgen@rwth-aachen.de; martin@rwth-aachen.de

Phone: +49 241 80 94712. Fax: +49 241 80 92128

Abstract

Sm doped ceria has one of the highest ionic conductivities reported for a rare-earth doped cerium oxide. The high oxygen ion conductivity can be attributed to the creation of oxygen vacancies by doping and weak defect interactions between oxygen vacancies and dopants. Especially, oxygen vacancies in nearest neighborhood to dopants decrease the conductivity due to trapping and blocking. In this work, the local structure around the Ce cations is investigated using extended X-ray absorption fine structure. The result-

ing coordination numbers of cerium coordinated by oxygen are only marginally larger than in a random oxygen vacancy distribution explaining the large ionic conductivity.

Introduction

Solid solutions of ceria (CeO_2) and rare-earth oxides (RE_2O_3) are known for their high oxygen ion conductivity. As a result, rare-earth doped ceria can be applied in energy conversion and storage as electrolyte in solid oxide fuel cells, electrolyzer cells and high temperature batteries.[1] The underlying mechanism determining the ionic conductivity in rare-earth doped ceria has been a topic of research for half a century.[2] In experiments, a correlation between ionic conductivity and dopant radius was found.[3–7] Theoretical investigations include analytical models,[8–11] semi-empirical[12–15] and *ab initio* calculations.[16–22] The high ionic conductivity can be attributed to both the creation of oxygen vacancies $V_O^{\bullet\bullet}$ by doping, as shown in Eq. 1 in Kröger-Vink notation,[23] and weak defect interactions.[2] The concentration of intrinsic- or reduction-dominated vacancies is significantly smaller as discussed in literature and can be neglected in this work.[24–26]

$$RE_2O_3 \longrightarrow 2\,RE'_{Ce} + 3\,O_O^{\times} + V_O^{\bullet\bullet} \tag{1}$$

Defect interactions include increased migration barriers for oxygen vacancy jumps around dopants (blocking).[22,27] Blocking appears at configurations where the two adjacent Ce cations along the migration pathway of the oxygen (migration edge, Fig. 1) are substituted by large rare-earth dopants.[15,22,28–30] Additionally, the association between dopants and oxygen vacancies increases migration barriers for oxygen jumps away from dopants (trapping) and decreased migration barriers for oxygen jumps towards dopants.[2,22] For Sm doped ceria, defect interactions are small compared to other rare-earth dopants resulting in the high oxygen ion conductivity as found in experiments[31–40] and our earlier simulations.[2,26,28] In our simulations, we predicted ionic conductivity using Kinetic Monte Carlo (KMC) simulations[41]

based on density functional theory (DFT) calculations, which are in excellent agreement with experiments.[2,42]

For an experimental proof and a better understanding of the weak defect interactions in Sm doped ceria, the average coordination number for the first shells around cerium ions, which contain oxygen ions, can be studied. Figure 1 shows that, for both blocking and trapping configurations, oxygen vacancies and Sm dopants appear in nearest neighborhood and, therefore, decrease the Ce-O coordination number. Structural properties can be investigated by X-Ray absorption spectroscopy (XAS) featuring the absorption edge or X-ray absorption near-edge structure (XANES) and extended X-ray absorption fine structure (EXAFS).

In literature, rare-earth doped ceria ($Ce_{1-x}RE_xO_{2-x/2}$) has already been studied using XANES[43] and EXAFS.[44–54] Hormes *et al.* investigated Pr, Gd, Ho, La, and Sm doped ceria ($x = 0.2$) and found in XANES measurements that the decreased conductivity in Nd and La doped ceria can be traced back to differences in the geometric structure.[43] For Gd doped ceria ($0 \leq x \leq 0.3$), Ohashi *et al.* inferred that cerium has the 4+ valence state and that Ce-O and Gd-O interatomic distances decrease with increasing dopant fraction due to defect association.[44] Yamazaki *et al.* confirmed the valence state of cerium in Sc, Y, Nd, Sm, Gd, and Yb doped ceria ($0 \leq x \leq 0.3$).[45] They also found decreasing Ce-O, Gd-O and Y-O interatomic distances with increasing dopant fraction, except for Sc where two phases are found. Yoshida *et al.* used the Ce-O interatomic distances to extract coordination numbers in Y,

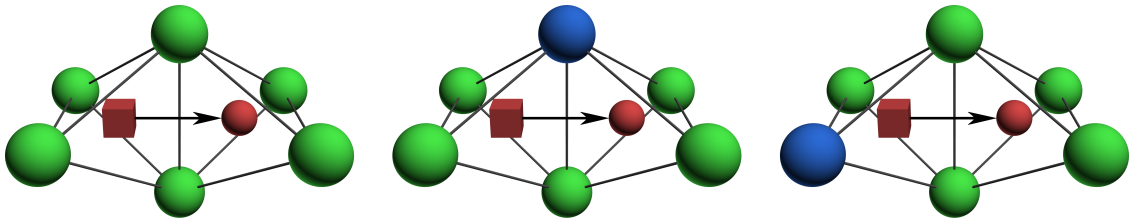

Figure 1: Possible migration configurations in samarium doped ceria. Ce-Ce migration edge (left), the blocking Ce-Sm migration edge (middle) and a trapped oxygen vacancy in nearest neighborhood to an Sm dopant (right). The appearance of blocking and trapping configurations increases the Ce-O coordination number and decreases the conductivity. Cerium ions (green), samarium ions (blue), oxygen ions (red spheres) and oxygen vacancies (red boxes).[28] - Reproduced by permission of the PCCP Owner Societies

Sm, Nd, and La doped ceria ($x = 0.2$), obtained high Ce-O coordination numbers compared to a random distribution and, therefore, confirmed the association of oxygen vacancies with dopants.[46] High uncertainties (± 1) for the coordination number directly extracted from the EXAFS oscillation for Gd, Y, and La doped ceria ($0.05 \leq x \leq 0.3$) were reported by Deguchi *et al.*[50] Finally, Wang *et al.* found no influence of the grain size on the local structure in Y doped ceria ($x = 0.18$).[51]

Sm doped ceria, however, which possesses the highest ionic conductivity,[2] has only been investigated for the dopant fractions $x = 0.1$, 0.2, and 0.3.[43,45–47] Coordination numbers are only reported for $Ce_{0.8}Sm_{0.2}O_{1.9}$. In this work, the coordination numbers for a detailed concentration series of Sm doped ceria ($\Delta x = 0.025$ for $Ce_{1-x}Sm_xO_{2-x/2}$) are given, and the method of calculating the coordination number is improved.

The paper is organized as follows: In section 2, details according to the experimental setup and data processing are described. In section 3, we present our results for the coordination number in pure and Sm doped ceria. Finally, we compare our results with experiments and simulations in literature. In section 4, we give a short summary.

Experimental details

Polycrystalline samples were prepared by dissolving cerium (III) nitrate hexahydrate (99.9%, Chempur), samarium nitrate hexahydrate (99.9 %, Sigma-Aldrich) and citric acid (VWR International, 2.5 equivalents) in water. During mixing for several hours at 50 °C the sol-gel transformation occurred. The temperature was increased to 350 °C where the produced foam was dried for three hours and subsequently calcined for four hours at 1000 °C. The calcined powder was dry milled in a planetary mill, uniaxially pressed to disks (10 mm in diameter and 2 mm thick) and sintered in air at 1400 °C for 24 hours with a heating and cooling rate of 200 °C/hour. The composition was successfully verified using X-Ray diffraction (Theta-Theta diffractometer, STOE, Darmstadt, Germany).[55] Density measurements according to

the Archimedes method gave high densities around 95% of the theoretical value.

X-Ray absorption measurements on ceria and Sm doped ceria were performed at the Ce(K)edge using CeO_2 as a reference. X-Rays were generated in the positron storage ring Doris III (DESY, Hamburg, Germany), where positrons were accelerated to an energy of 4.5 GeV. Experiments were performed in HASYLAB at Beamline C using a Si (311) single crystal couple monochromator. Intensities were measured using gas ionization chambers for crushed samples mixed with boron nitride and, alternatively, as X-Ray fluorescence for pellets using a Passivated Implanted Planar Silicon detector (PIPS) with 75 mm diameter.[56,57]

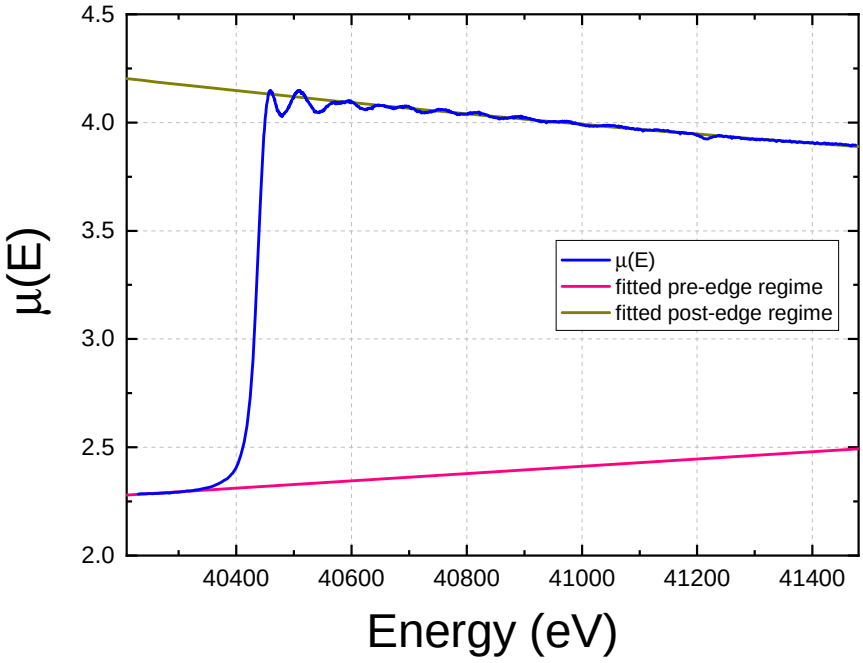

Figure 2: Absorption coefficient at Ce(K)-edge of 2.5 % Sm doped ceria as a function of the incident X-Ray energy.

The XAS data was processed using the program Athena[58] by fitting of the pre- and post-edge regime (Fig. 2) and normalization of the absorption coefficient. No change in the valence state for the cerium cations at room temperature is found in agreement with literature.[44–46] Therefore, an energy alignment of the absorption edge to the reference sample CeO_2 is performed.

The local structure can be investigated by transforming the EXAFS region of the absorp-

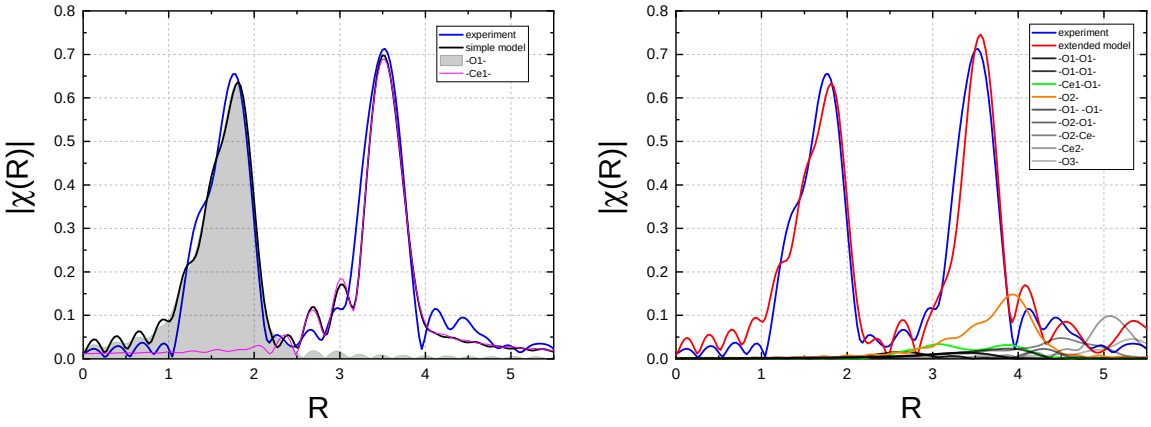

Figure 3: Modeling an EXAFS measurement of 2.5 % Sm doped ceria. Right: Simple model with two scattering paths in comparison with the experimental result. Left: Minor improvement in an extended model using 11 paths.

tion coefficient into a modified Radial Distribution Function. For this purpose, a background removal using a spline function according to literature[59] and the transformation from the energy into the wave vector-range according to Eq. 2 with the the inflection point E_0 and the electron mass m_e are performed.

$$k = \sqrt{2m_e \left(E - E_0\right) / \hbar^2} \tag{2}$$

For larger energies or wave vectors, the EXAFS oscillations decay. Therefore, $\chi\left(k\right)$ is weighted with k^2 in this work. The k^n-weighted EXAFS oscillations as a function of the wave vector $k^n\chi\left(k\right)$ can be transformed into a pair correlation function or Modified Radial Distribution Function (RDF)[1] in the direct space $\left|\chi\left(R\right)\right|$ using a Forward Fourier transform according to Eq. 3 (Fig. 3).[60,61] For this purpose, only a limited k-range similar for all samples is selected by applying a window function $W\left(k\right)$ between about 2–11 Å^{-1} depending on the signal-to-noise ratio.

$$\chi\left(R\right) = \frac{1}{\sqrt{2\pi}} \int_{k_{\min}}^{k_{\max}} k^n \cdot \chi\left(k\right) \cdot W\left(k\right) \cdot \mathrm{e}^{2ikR} \mathrm{d}k \tag{3}$$

[1] In contrast to a pair correlation function, $\left|\chi\left(R\right)\right|$ still possess a phase shift δ_i for the different scattering paths, which is corrected by fitting with the EXAFS equation.

For pure and doped ceria, the Radial Distribution Function around a cation (Fig. 3) shows contributions of oxygen ions (first peak) as well as cerium ions or rare-earth dopants (second peak). In this work, the distribution of the oxygen vacancies is investigated. Therefore, the occupation of the first coordination shell is of particular interest and can be investigated by modeling the EXAFS oscillation.

As the structure of the pure and doped ceria ($Fm\bar{3}m$) is well known,[7,23,62] $\chi(k)$ can be modeled using the EXAFS equation and fitted to the experimental data. The EXAFS oscillation was modeled using the program Artemis[58] and IFEFFIT.[63] The sinusoidal oscillation in the absorption coefficient is damped by the limited lifetime of the excited photoelectron that is scattered both elastically and inelastically and the thermal and statistical disorder. The EXAFS equation calculates $\chi(k)$ as a sum of multiple scattering paths $\chi(k) = \sum_i \chi_i(k)$ with

$$\chi_i(k) = \frac{N_i S_0^2}{k R_i^2} F_i(k) \sin\left[2kR_i + \delta_i(k)\right] \mathrm{e}^{-2\sigma_i^2 k^2} \mathrm{e}^{-2R_i/\lambda(k)} \tag{4}$$

$$\text{using } N_i S_0^2 = amp_i \cdot N_0,\ k = \sqrt{2m_\mathrm{e}(E - E_0)/\hbar^2} \tag{5}$$

$$\text{and } R_i = R_0 + \Delta R_i. \tag{6}$$

For the crystalline ceria structure, the distance to the scattering atom in pure ceria R_0 and the sample-independent degeneracy of path N_0 are given by the structure. The effective scattering amplitude F_i, the effective scattering phase shift δ_i and the mean free path $\lambda(k)$ were calculated using the *ab initio* program code FEFF8.[64] A ceria reference sample can be used to determine the energy shift E_0 and the mean squared displacement σ_i^2. Therefore, only the amplitude amp_i and the change in distance to the scattering atom ΔR_i for each path are the fitted parameters for each sample. The local structure is given by N_i and R_i which show the number and distance of neighboring atoms.

To model the EXAFS oscillation only a limited number of scattering paths, which contribute in the investigated R-region, is selected. Figure 3 shows the Radial Distribution Function of 2.5 % Sm doped ceria with (a) two and (b) 11 fitted scattering paths. The simple

model in (a) uses only the two scattering paths that possess amplitudes ten times bigger than nearly all other paths in the (b) extended model. As the difference in the Radial Distribution Function and the parameters of both models is small, only the two main scattering paths are considered in this work.

Results and Discussion

The Radial Distribution Function is extracted from the EXAFS oscillation for the series $Ce_{1-x}Sm_xO_{2-x/2}$ with $\Delta x = 0.025$. For the Ce-edge in Sm doped ceria, the extracted Radial Distribution Function before phase-shift correction is shown in Fig. 4. The Radial Distribution Function shows contributions of oxygen ions or vacancies (first peak) as well as cerium ions or Sm dopants (second peak). The amplitude fluctuates for the first coordination shell. For the second coordination shell, the amplitude decreases with increasing dopant fraction and changes its shape. Similar observations were made previously.[46,51,52,65] For Y, Gd and La doped ceria, even a decrease for the amplitude of the first peak with increasing dopant fraction up to $x = 0.25$ was found.[44,45,50]

Compared to pure ceria, doping with Sm leads to smaller amplitudes due to a decrease in coordination number and an increase in structural disorder. For the first peak, especially a decrease in coordination number is expected. In this work, however, only a fluctuation of the amplitude can be observed. For the second peak, an increasing amount of Sm dopants clearly leads to lower backscattering. The Debye-Waller factor decreases due to the disorder of the cation sublattice caused by the cation substitution. The increasing disorder also contributes to the broadening of the second peak.

Additionally, differences in interatomic distance can be observed. The maximum of the first coordination peak (oxygen ions and vacancies) moves to lower R values for higher dopant fractions. The second peak broadens and rather moves to larger R values for higher dopant fractions. Similar observations were made up to $x = 0.2$ in literature, though the

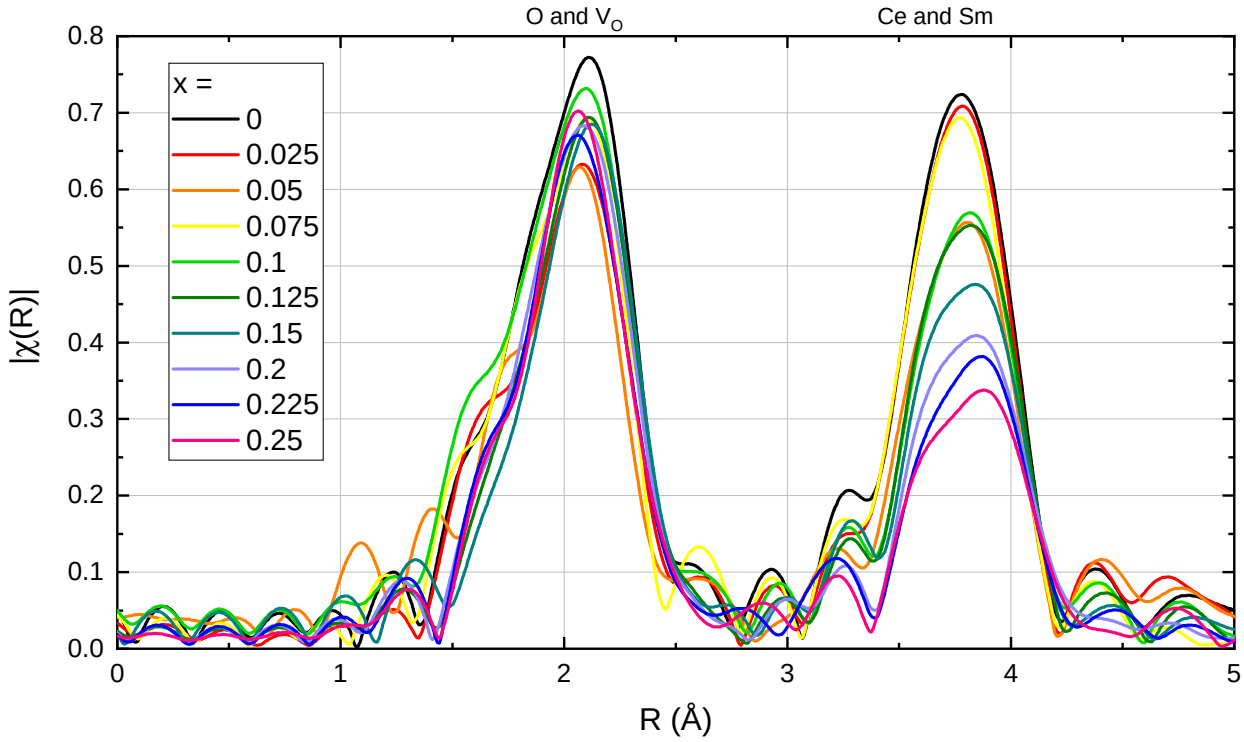

Figure 4: Radial Distribution Function at Ce(K)-edge of $Ce_{1-x}Sm_xO_{2-x/2}$.

position of the second peak varies.[44–46,50–52,65] An exception is the result of Yamazaki *et al.*[45] They show in the Radial Distribution Function for the maximum of the first peak an increasing R value with increasing dopant fraction, though they report decreasing Ce-O distances.[45] The reason for this deviation is the missing phase-shift correction for the shown Radial Distribution Function. This emphasizes the importance of modeling according to the EXAFS equation.

Decreasing Ce-O distances correlate with the expected decrease in coordination number. In other words, oxygen ions near cations relax towards adjacent vacancies leading to decreasing cation-anion distances. Especially the position of the second peak is influenced by the change in lattice parameter.[2,31,66] As the distances between Ce-Ce and Ce-dopant differ, a broadening of the second peak is observed as shown by Deguchi *et al.*[50]

In the next step, the Radial Distribution Function is modeled using the EXAFS equation. The results are shown in Table 1. To investigate the local structure, the first coordination shell around a cation was chosen. Here, oxygen ions or vacancies are present. The occupation

Table 1: Fit results of the EXAFS data of $Ce_{1-x}Sm_xO_{2-x/2}$ at the Ce-edge. The amplitude amp_i and the distance to the scattering ion R_i is shown.

x	amp_i		R_i (Å)	
	1st shell	2nd shell	1st shell	2nd shell
0	0.89(4)	0.93(5)	2.338(4)	3.859(3)
0.025	0.64(5)	0.85(6)	2.356(6)	3.870(4)
0.05	0.62(4)	0.66(5)	2.336(5)	3.862(4)
0.075	0.70(5)	0.84(6)	2.348(5)	3.865(3)
0.1	0.72(4)	0.68(5)	2.335(4)	3.859(3)
0.125	0.65(4)	0.68(5)	2.341(5)	3.863(4)
0.15	0.61(4)	0.60(5)	2.329(5)	3.860(4)
0.2	0.63(4)	0.50(5)	2.323(5)	3.853(5)
0.225	0.60(4)	0.45(5)	2.319(5)	3.853(6)
0.25	0.61(4)	0.40(5)	2.312(5)	3.848(6)

of the first coordination shell or the coordination number of cations shows the formation of Ce-V or Sm-V associates in nearest neighborhood. For a random distribution of defects, the (average) coordination number is

$$\mathrm{CN} = 8 - 2 \cdot x. \tag{7}$$

The oxygen vacancy concentration increases for increasing dopant fractions leading to a lower coordination number for the first shell of Ce^{4+} ions. A random distribution will emerge at very high temperatures. A general decrease in Ce-O coordination number with increasing dopant fraction was already shown previously in rare-earth doped ceria.[44,45,50]

The coordination number can directly be extracted from the EXAFS equation from the amplitude. For the amplitude, the coordination number is

$$\mathrm{CN}_i = 8 \cdot \frac{amp_i}{amp\,(\mathrm{CeO_2})}. \tag{8}$$

The coordination number is equivalent to the number of neighboring atoms N, which is fitted here with the amplitude. However, the amplitude depends strongly on the EXAFS Data Processing and has a great error, which can be seen in Fig. 5. Using the amplitude in the EXAFS equation additionally leads to a poor approximation of the Ce-O coordination

number. Ce-O coordination numbers are significantly lower than predicted by a random cation distribution. This would mean that oxygen vacancies do not associate with rare-earth dopants but appear near cerium ions. While this might be a reason for further investigations, in fact, the Ce-O coordination numbers are lower than even physically possible as determined by the oxygen vacancy concentration.

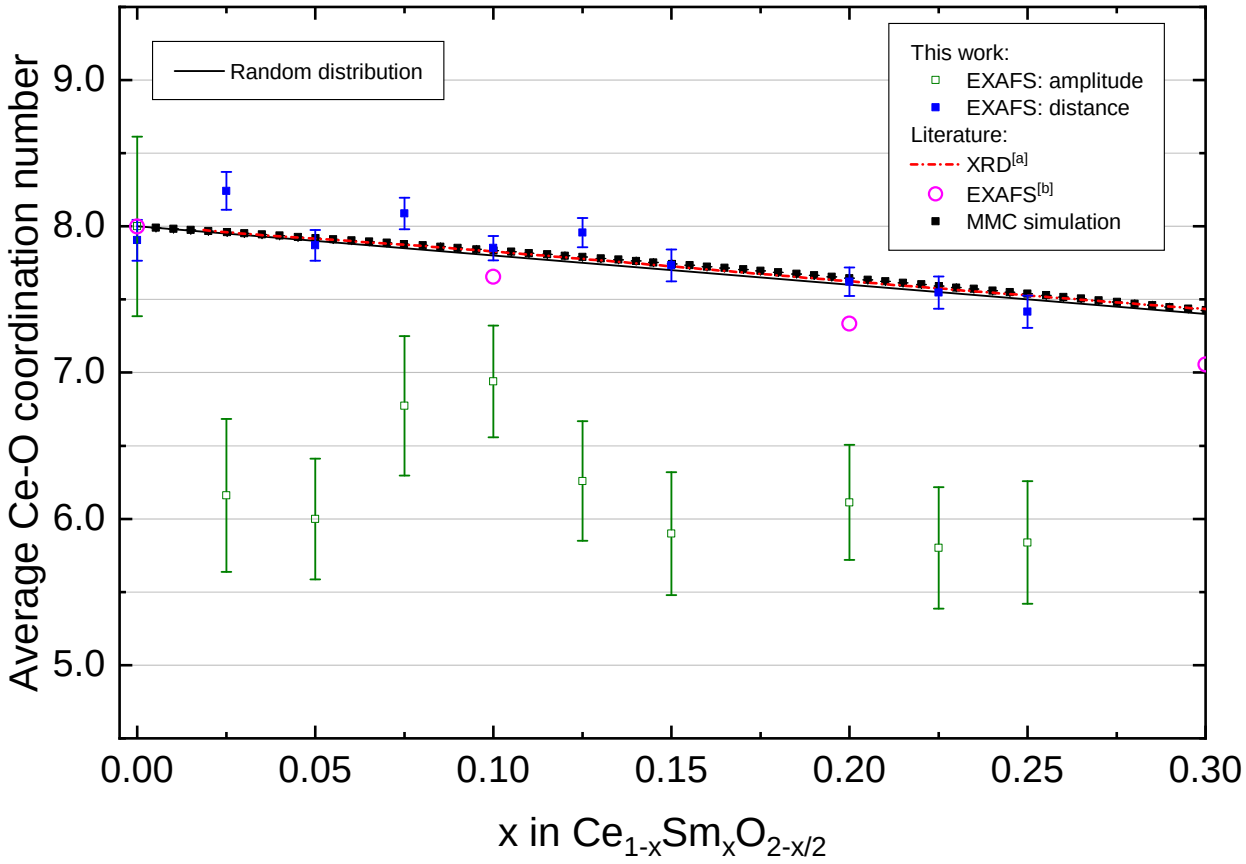

Figure 5: Coordination number of Ce-O for Sm doped ceria. X-ray diffraction experiments according to Nakamura [a].[67] EXAFS experiments according to Eq. 9 using data from Yamazaki *et al.* [b].[45] Metropolis Monte Carlo simulations according to an earlier work.[28]

Alternatively, the determination of the coordination number can be improved by using the distance to the neighboring atoms R. Shannon has shown that the ionic radius depends on the coordination number.[68] According to Shannon, the distance between cation and anion lattice sites decreases for an increasing number of vacant anion lattice sites (or for a lower coordination number). Therefore, a coordination number can be calculated from the distance

to the neighboring atom (Fig. 5). For the distance, the coordination number is

$$\mathrm{CN}_i = 6 + 2 \cdot \frac{r_i - r^{\mathrm{CN}=6}}{r^{\mathrm{CN}=8} - r^{\mathrm{CN}=6}}, \tag{9}$$

with the distances $r^{\mathrm{CN}=6}$ and $r^{\mathrm{CN}=8}$ given by Shannon,[68] which are shifted to the Ce-O distance according to X-ray diffraction measurements in pure ceria.[23] For the latter, $\mathrm{CN} = 6$ is the only investigated coordination number smaller than $\mathrm{CN} = 8$. In this simple model, a mixture of the two isotropic coordination states is assumed. The error of the coordination number based on the distances is significantly smaller than for the amplitude (Fig. 5). Comparing both types of coordination numbers suggests that the error based on the EXAFS fitting procedure is smaller than the actual systematic error of the data, especially for the amplitude data.

Using the distance leads to a significantly better coordination number in the range of both random distribution and X-ray diffraction measurements by Nakamura.[67] Moreover, in this work, we significantly improved the measured coordination numbers compared to results extracted from the interatomic distances reported by Yamazaki *et al.*[45] The slight increase in Ce-O coordination number compared to the random distribution is caused by the association of Sm dopants and oxygen vacancy (trapping). As the deviation to the random distribution is marginal, the Sm-V association is weak in Sm doped ceria. This is also confirmed by the agreement with our earlier Metropolis Monte Carlo simulations based on density functional theory calculations.[28] While the EXAFS measurements were performed at room temperature, doped ceria is applied in applications that often have significantly higher operating temperatures. At higher temperatures, the fraction of oxygen vacancies that are trapped by dopants is even lower due to the increase in available thermal energy.

In our earlier work, we demonstrated that the activation barriers for oxygen ion migration depend on the oxygen vacancy trapping on the one hand, and on an energy contribution depending on the migration edge (Fig. 1, blocking) on the other. Kinetic Monte Carlo sim-

ulations were applied to simulate the oxygen ion conductivity and the selective deactivation of both energy contributions allowed a deeper understanding of the influence of the blocking and trapping effect on the ionic conductivity. We demonstrated that the low trapping effect in Sm doped ceria results in a high oxygen ion conductivity.[2] In this work, the coordination numbers determined by EXAFS give us a direct insight in the oxygen vacancy trapping that directly determines the low migration barriers and the high ionic conductivity in Sm doped ceria.

Conclusions

Coordination numbers in Sm doped ceria were determined using X-Ray absorption in agreement with experiments and simulations. The accuracy of the coordination numbers from extended X-ray absorption fine structure (EXAFS) experiments for the Ce-edge in Sm doped ceria was improved compared to studies considering only the amplitude of the Radial Distribution Function as well as studies reporting Ce-O interatomic distances. The association of oxygen vacancies and Sm dopants was verified. Only small defect interactions were shown by similar coordination numbers in Sm dopant ceria and a random distribution of defects providing a new physical insight in the microscopic origin of the high macroscopic ionic conductivity in Sm doped ceria.

Acknowledgement

The authors thank Roman Chernikov from HASYLAB (DESY, Hamburg), Milias Liu, Thomas Beckers and Henning Schraknepper for their support during the EXAFS beam time. The authors gratefully acknowledge the computing time granted by the JARA-HPC Vergabegremium and provided on the JARA-HPC Partition part of the supercomputer JURECA at Forschungszentrum Jülich.[69] Simulations were performed with computing resources granted by RWTH Aachen University under project rwth0336. The authors gratefully acknowledge the com-

puting time granted by the JARA-HPC Vergabegremium and provided on the JARA-HPC Partition part of the supercomputer CLAIX at RWTH Aachen University. Research supported by the U.S. Department of Energy, Office of Science, Basic Energy Sciences, Materials Sciences and Engineering Division under Contract No. DE-AC02-05-CH11231.

References

(1) Steele, B. C. H.; Heinzel, A. Materials for fuel-cell technologies. *Nature* **2001**, *414*, 345–352.

(2) Koettgen, J.; Grieshammer, S.; Hein, P.; Grope, B. O. H.; Nakayama, M.; Martin, M. Understanding the ionic conductivity maximum in doped ceria: trapping and blocking. *Phys. Chem. Chem. Phys.* **2018**, *20*, 14291–14321.

(3) Wang, D.; Park, D.; Griffith, J.; Nowick, A. Oxygen-ion conductivity and defect interactions in yttria-doped ceria. *Solid State Ionics* **1981**, *2*, 95–105.

(4) Yahiro, H. Electrical properties and reducibilities of ceria-rare earth oxide systems and their application to solid oxide fuel cell. *Solid State Ionics* **1989**, *36*, 71–75.

(5) Eguchi, K.; Setoguchi, T.; Inoue, T.; Arai, H. Electrical properties of ceria-based oxides and their application to solid oxide fuel cells. *Solid State Ionics* **1992**, *52*, 165–172.

(6) Mogensen, M.; Lindegaard, T.; Hansen, U. R.; Mogensen, G. Optimizing mixed conductor SOFC anodes of doped CeO_2. Proceedings of the Second International Symposium on Ionic and Mixed Conducting Ceramics. Pennington, NJ, 1994; pp 448–465.

(7) Inaba, H.; Tagawa, H. Ceria-based solid electrolytes. *Solid State Ionics* **1996**, *83*, 1–16.

(8) Strickler, D. W.; Carlson, W. G. Electrical conductivity in the ZrO_2-rich region of several M_2O_3-ZrO_2 systems. *J. Am. Ceram. Soc.* **1965**, *48*, 286–289.

(9) Schmalzried, H. On correlation effects of vacancies in ionic crystals. *Z. Phys. Chem.* **1977**, *105*, 47–62.

(10) Hohnke, D. K. Ionic conduction in doped oxides with the fluorite structure. *Solid State Ionics* **1981**, *5*, 531–534.

(11) Martin, M. On the ionic conductivity of strongly acceptor doped, fluorite-type oxygen ion conductors. *J. Electroceram.* **2006**, *17*, 765–773.

(12) Catlow, C. R.; Parker, S. C. In *Computer Simulation of Solids*; Catlow, C., Mackrodt, W., Eds.; Lecture Notes in Physics; Springer Berlin Heidelberg, 1982; Vol. 166; pp 222–242.

(13) Butler, V.; Catlow, C.; Fender, B.; Harding, J. Dopant ion radius and ionic conductivity in cerium dioxide. *Solid State Ionics* **1983**, *8*, 109–113.

(14) Catlow, C. Transport in doped fluorite oxides. *Solid State Ionics* **1984**, *12*, 67–73.

(15) Murray, A.; Murch, G.; Catlow, C. A new hybrid scheme of computer simulation based on Hades and Monte Carlo: Application to ionic conductivity in Y^{3+} doped CeO2. *Solid State Ionics* **1986**, *18-19*, 196–202.

(16) Skorodumova, N. V.; Baudin, M.; Hermansson, K. Surface properties of CeO_2 from first principles. *Phys. Rev. B* **2004**, *69*, 075401.

(17) Yang, Z.; Woo, T. K.; Baudin, M.; Hermansson, K. Atomic and electronic structure of unreduced and reduced CeO_2 surfaces: A first-principles study. *J. Chem. Phys.* **2004**, *120*, 7741.

(18) Andersson, D. A.; Simak, S. I.; Skorodumova, N. V.; Abrikosov, I. A.; Johansson, B. Optimization of ionic conductivity in doped ceria. *Proc. Natl. Acad. Sci. U.S.A.* **2006**, *103*, 3518–3521.

(19) Ismail, A.; Hooper, J.; Giorgi, J. B.; Woo, T. K. A DFT+U study of defect association and oxygen migration in samarium-doped ceria. *Phys. Chem. Chem. Phys.* **2011**, *13*, 6116.

(20) Chroneos, A.; Yildiz, B.; Tarancón, A.; Parfitt, D.; Kilner, J. A. Oxygen diffusion in solid oxide fuel cell cathode and electrolyte materials: Mechanistic insights from atomistic simulations. *Energy Environ. Sci.* **2011**, *4*, 2774.

(21) Lucid, A. K.; Keating, P. R. L.; Allen, J. P.; Watson, G. W. Structure and reducibility of CeO_2 doped with trivalent cations. *J. Phys. Chem. C* **2016**, *120*, 23430–23440.

(22) Fu, Z.; Sun, Q.; Ma, D.; Zhang, N.; An, Y.; Yang, Z. Effects of Sm doping content on the ionic conduction of CeO_2 in SOFCs from first principles. *Appl. Phys. Lett.* **2017**, *111*, 023903.

(23) Mogensen, M.; Sammes, N. M.; Tompsett, G. A. Physical, chemical and electrochemical properties of pure and doped ceria. *Solid State Ionics* **2000**, *129*, 63–94.

(24) Tuller, H. L. Defect structure and electrical properties of nonstoichiometric CeO_2 single crystals. *J. Electrochem. Soc.* **1979**, *126*, 209.

(25) Zacherle, T.; Schriever, A.; De Souza, R. A.; Martin, M. Ab initio analysis of the defect structure of ceria. *Phys. Rev. B* **2013**, *87*, 134104.

(26) Koettgen, J.; Zacherle, T.; Grieshammer, S.; Martin, M. Ab initio calculation of the attempt frequency of oxygen diffusion in pure and samarium doped ceria. *Phys. Chem. Chem. Phys.* **2017**, *19*, 9957–9973.

(27) Koettgen, J.; Schmidt, P. C.; Bučko, T.; Martin, M. Ab initio calculation of the migration free energy of oxygen diffusion in pure and samarium-doped ceria. *Phys. Rev. B* **2018**, *97*, 024305.

(28) Grieshammer, S.; Grope, B. O. H.; Koettgen, J.; Martin, M. A combined DFT + U and Monte Carlo study on rare earth doped ceria. *Phys. Chem. Chem. Phys.* **2014**, *16*, 9974.

(29) Grieshammer, S.; Eisele, S.; Koettgen, J. Modeling oxygen ion migration in the CeO_2–ZrO_2–Y_2O_3 solid solution. *J. Phys. Chem. C* **2018**, *122*, 18809–18817.

(30) Koettgen, J.; Dück, G.; Martin, M. The ionic conductivity of Lu doped ceria. *in preparation*

(31) Zhan, Z.; Wen, T.-L.; Tu, H.; Lu, Z.-Y. AC impedance investigation of samarium-doped ceria. *J. Electrochem. Soc.* **2001**, *148*, A427.

(32) Sanghavi, R.; Devanathan, R.; Nandasiri, M. I.; Kuchibhatla, S.; Kovarik, L.; Thevuthasan, S.; Prasad, S. Integrated experimental and modeling study of the ionic conductivity of samaria-doped ceria thin films. *Solid State Ionics* **2011**, *204-205*, 13–19.

(33) Bellino, M. G.; Lamas, D. G.; Walsöe de Reca, N. E., Enhanced ionic conductivity in nanostructured, heavily doped ceria ceramics. *Adv. Funct. Mater.* **2006**, *16*, 107–113.

(34) Omar, S.; Wachsman, E. D.; Jones, J. L.; Nino, J. C. Crystal structure-ionic conductivity relationships in doped ceria systems. *J. Am. Ceram. Soc.* **2009**, *92*, 2674–2681.

(35) Pérez-Coll, D.; Marrero-López, D.; Núñez, P.; Piñol, S.; Frade, J. R. Grain boundary conductivity of $Ce_{0.8}Ln_{0.2}O_{2-\delta}$ ceramics (Ln=Y, La, Gd, Sm) with and without Co-doping. *Electrochim. Acta* **2006**, *51*, 6463–6469.

(36) van Herle, J.; Seneviratne, D.; McEvoy, A. Lanthanide co-doping of solid electrolytes: AC conductivity behaviour. *J. Eur. Ceram. Soc.* **1999**, *19*, 837–841.

(37) Van herle, J.; Horita, T.; Kawada, T.; Sakai, N.; Yokokawa, H.; Dokiya, M. Low temperature fabrication of (Y,Gd,Sm)-doped ceria electrolyte. *Solid State Ionics* **1996**, *86-88*, 1255–1258.

(38) Zheng, Y.; Zhou, M.; Ge, L.; Li, S.; Chen, H.; Guo, L. Effect of Dy on the properties of Sm-doped ceria electrolyte for IT-SOFCs. *J. Alloys Compd.* **2011**, *509*, 1244–1248.

(39) Zajac, W.; Molenda, J. Electrical conductivity of doubly doped ceria. *Solid State Ionics* **2008**, *179*, 154–158.

(40) Koettgen, J.; Peters, L.; Martin, M. The ionic conductivity of Sm doped ceria. *in preparation*

(41) Hein, P.; Grope, B. O. H.; Koettgen, J.; Grieshammer, S.; Martin, M. iCon: A general lattice Kinetic Monte Carlo program. *submitted*

(42) Koettgen, J.; Martin, M. The effect of entropy on the ionic conductivity in doped ceria. *in preparation*

(43) Hormes, J.; Pantelouris, M.; Balazs, G. B.; Rambabu, B. X-ray absorption near edge structure (XANES) measurements of ceria-based solid electrolytes. *Solid State Ionics* **2000**, *136-137*, 945–954.

(44) Ohashi, T.; Yamazaki, S.; Tokunaga, T.; Arita, Y.; Matsui, T.; Harami, T.; Kobayashi, K. EXAFS study of $Ce_{1-x}Gd_xO_{2-x/2}$. *Solid State Ionics* **1998**, *113-115*, 559–564.

(45) Yamazaki, S.; Matsui, T.; Ohashi, T.; Arita, Y. Defect structures in doped CeO_2 studied by using XAFS spectrometry. *Solid State Ionics* **2000**, *136-137*, 913–920.

(46) Yoshida, H.; Deguchi, H.; Miura, K.; Horiuchi, M.; Inagaki, T. Investigation of the relationship between the ionic conductivity and the local structures of singly and doubly doped ceria compounds using EXAFS measurement. *Solid State Ionics* **2001**, *140*, 191–199.

(47) Yamazaki, S.; Matsui, T.; Sato, T.; Arita, Y.; Nagasaki, T. EXAFS study of reduced ceria doped with lanthanide oxides. *Solid State Ionics* **2002**, *154-155*, 113–118.

(48) Deganello, F.; Longo, A.; Martorana, A. EXAFS study of ceria–lanthana-based TWC promoters prepared by sol–gel routes. *J. Solid State Chem.* **2003**, *175*, 289–298.

(49) Nitani, H.; Nakagawa, T.; Yamanouchi, M.; Osuki, T.; Yuya, M.; Yamamoto, T. A. XAFS and XRD study of ceria doped with Pr, Nd or Sm. *Mater. Lett.* **2004**, *58*, 2076–2081.

(50) Deguchi, H.; Yoshida, H.; Inagaki, T.; Horiuchi, M. EXAFS study of doped ceria using multiple data set fit. *Solid State Ionics* **2005**, *176*, 1817–1825.

(51) Wang, Y.; Kageyama, H.; Mori, T.; Yoshikawa, H.; Drennan, J. Local structures around Y and Ce cations in 10 mol% Y_2O_3 doped ceria ceramics by EXAFS spectroscopy. *Solid State Ionics* **2006**, *177*, 1681–1685.

(52) Chadwick, A. V.; Savin, S. L. EXAFS study of nanocrystalline CeO_2 samples prepared by sol–gel and ball-milling routes. *J. Alloys Compd.* **2009**, *488*, 1–4.

(53) Korobko, R.; Lerner, A.; Li, Y.; Wachtel, E.; Frenkel, A. I.; Lubomirsky, I. In-situ extended X-ray absorption fine structure study of electrostriction in Gd doped ceria. *Appl. Phys. Lett.* **2015**, *106*, 042904.

(54) Li, Y.; Kraynis, O.; Kas, J.; Weng, T.-C.; Sokaras, D.; Zacharowicz, R.; Lubomirsky, I.; Frenkel, A. I. Geometry of electromechanically active structures in gadolinium - doped cerium oxides. *AIP Adv.* **2016**, *6*, 055320.

(55) Leichtweiss, T.; Henning, R. A.; Koettgen, J.; Schmidt, R. M.; Holländer, B.; Martin, M.; Wuttig, M.; Janek, J. Amorphous and highly nonstoichiometric titania (TiO_x) thin films close to metal-like conductivity. *J. Mater. Chem. A* **2014**, *2*, 6631.

(56) Mueller, D. N.; De Souza, R. A.; Brendt, J.; Samuelis, D.; Martin, M. Oxidation states of the transition metal cations in the highly nonstoichiometric perovskite-type oxide $Ba_{0.1}Sr_{0.9}Co_{0.8}Fe_{0.2}O_{3-\delta}$. *J. Mater. Chem.* **2009**, *19*, 1960.

(57) Liu, M.; Leichtweiß, T.; Janek, J.; Martin, M. In-situ structural investigation of non-stoichiometric HfO_{2-x} films using quick-scanning extended X-ray absorption fine structure. *Thin Solid Films* **2013**, *539*, 60–64.

(58) Ravel, B.; Newville, M. ATHENA, ARTEMIS, HEPHAESTUS: data analysis for X-ray absorption spectroscopy using IFEFFIT. *J. Synchrotron Radiat.* **2005**, *12*, 537–541.

(59) Newville, M.; Livinš, P.; Yacoby, Y.; Rehr, J. J.; Stern, E. A. Near-edge X-ray-absorption fine structure of Pb: A comparison of theory and experiment. *Phys. Rev. B* **1993**, *47*, 14126–14131.

(60) Koningsberger, D. C.; Mojet, B. L.; van Dorssen, G. E.; Ramaker, D. E. XAFS spectroscopy; fundamental principles and data analysis. *Top. Catal.* **2000**, *10*, 143–155.

(61) Sayers, D. E.; Stern, E. A.; Lytle, F. W. New technique for investigating noncrystalline structures: fourier analysis of the extended X-ray—absorption fine structure. *Phys. Rev. Lett.* **1971**, *27*, 1204–1207.

(62) Hahn, T., Ed. *International tables for crystallography*, 5th ed.; Springer Netherland: Berlin, 2007.

(63) Rehr, J. J.; Albers, R. C.; Zabinsky, S. I. High-order multiple-scattering calculations of X-ray-absorption fine structure. *Phys. Rev. Lett.* **1992**, *69*, 3397–3400.

(64) Rehr, J. J.; Albers, R. C. Theoretical approaches to X-ray absorption fine structure. *Rev. Mod. Phys.* **2000**, *72*, 621–654.

(65) Li, P.; Chen, I.-W.; Penner-Hahn, J. E.; Tien, T.-Y. X-ray absorption studies of ceria with trivalent dopants. *J. Am. Ceram. Soc.* **1991**, *74*, 958–967.

(66) Zha, S.; Xia, C.; Meng, G. Effect of Gd (Sm) doping on properties of ceria electrolyte for solid oxide fuel cells. *J. Power Sources* **2003**, *115*, 44–48.

(67) Nakamura, A. New defect-crystal-chemical approach to non-Vegardianity and complex defect structure of fluorite-based MO_2–$LnO_{1.5}$ solid solutions (M^{4+}=Ce, Th; Ln^{3+}=lanthanide), Part II: Detailed local-structure and ionic-conductivity analysis. *Solid State Ionics* **2010**, *181*, 1631–1653.

(68) Shannon, R. D. Revised effective ionic radii and systematic studies of interatomic distances in halides and chalcogenides. *Acta Crystallogr., Sect. A* **1976**, *32*, 751–767.

(69) Jülich Supercomputing Centre, JURECA: General-purpose supercomputer at Jülich Supercomputing Centre. *Journal of large-scale research facilities* **2016**, *2*, A62.

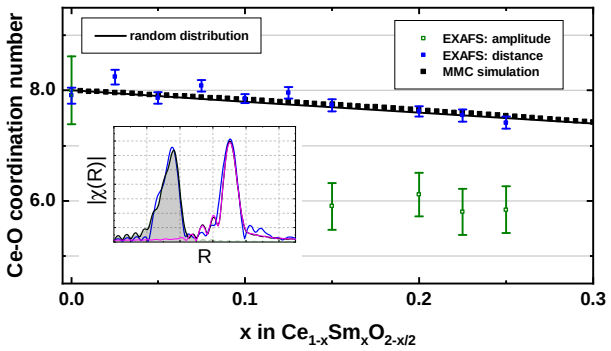

Figure 6: TOC Graphic